

Spectral characteristics of deforestation fires in NOAA/AVHRR images

M. C. PEREIRA and A. W. SETZER

Department of Remote Sensing and Satellite Meteorology,
Instituto Nacional de Pesquisas Espaciais, INPE/DSM, C. Postal 515,
S. J. Campos, SP, Brazil, 12201

(Received 29 April 1991; in final form 10 December 1991)

Abstract. This work presents optical-spectral and radiometric characteristics of fires associated to tropical deforestation as recorded by full resolution AVHRR/NOAA-9 images in the Amazon region during a dry season. Results showed that fires and smoke clouds were spectrally distinct and easily separated from surrounding ground covers by automatic digital processing. Channel 3 (3.55 to 3.93 μm) was the most appropriate to identify active fires whose pixels had digital counts about one order of magnitude higher than common ground covers.

1. Introduction

The use of the AVHRR (Advanced Very High Resolution Radiometer) on-board satellites of the NOAA-series (National Oceanic and Atmospheric Administration) to detect smoke plumes was first reported by Ernst and Matson (1977). They detected forest fire plumes on NOAA-5 images that originated in Canada and spread over the Bering Strait. Dozier (1981), Matson and Dozier (1981) and Matson *et al.* (1984) demonstrated that channel 3 (3.55 to 3.93 μm) of the NOAA polar orbiters could be used to detect forest fires over extensive regions. They also proposed that sizes of fires and even their temperatures could be obtained combining channels 3 and 4 (10.3–11.3 μm) if the AVHRR pixels were not saturated. Chung and Le (1984) used NOAA-7 imagery to identify forest fire plumes in West Canada in 1981, which were advected for 3000 km or even 5000 km over east North America, and covered areas over $1.2 \times 10^6 \text{ km}^2$. Svejkovsky (1985) detected in channel 1 (0.55 to 0.68 μm) and 2 (0.75 to 1.1 μm) of NOAA-6 images large smoke clouds possibly associated with large forest fires in California, some 1100 km away. Flannigan (1985) and Flannigan and Haar (1986) detected forest fires in Alberta, Canada, also with NOAA satellites and stressed the low cost and satisfactory spatial and temporal resolution of the technique. Malingreau (1984) and Malingreau *et al.* (1985) used NOAA-7 images to detect and map forest fires in Indonesia and Borneo in 1982–83, and showed that 'vegetation indexes' obtained through AVHRR channels 1 and 2 can be used to evaluate the extension and damage of the fires. Muirhead and Cracknell (1985) were able to detect with channel 3 of AVHRR 300–400 fires from straw and stubble burning in Great Britain. Fires near Manaus, in the Brazilian Amazonia, have been located by Matson and Holben (1987) with the same technique, and they suggested the use of AVHRR data to monitor fires on a global scale. Examples of fire detection in many parts of the world are found in Matson *et al.* (1987). AVHRR data was also used to assess the extensive fires in the Yellowstone Park (EOSAT 1988).

More recently, another example of AVHRR algorithm to detect fires was proposed by Lee and Tag (1990), and an extensive review of orbital remote sensing detection of fire was done by Robinson (1991). Concerning effects of biomass burning in the atmosphere (Crutzen and Andreae 1990), AVHRR has also started to play a significant role. Andreae *et al.* (1988) were able to show that haze layers over Amazonia originated from deforestation fires detected by AVHRR. Kirchoff *et al.* (1989) related the seasonality of ground measurements of ozone concentrations in Central Brazil to emissions from biomass burning detected in AVHRR channel 3, and Setzer *et al.* (1991) related the number of fires in channel 3 to tropospheric ozone variations measured in an aeroplane during the 'burning season' of Brazil. The amazing amount of such fires, of more than 350,000 in the dry year of 1987, has been estimated with AVHRR (Setzer and Pereira 1991 a). Kaufman *et al.* (1990) discussed more techniques to estimate emissions from biomass burning in Amazonia based on AVHRR images also for 1987.

The objective of the present work was to determine optical-spectral and radiometric characteristics of fires associated to tropical deforestation in Brazil as registered by the AVHRR imaging instrument of the NOAA-series satellites. These fires do not occur naturally in the Amazon forest, and they only burn what was cut a few months before and let dry. Information about such fires is needed considering alarming rates of forest conversion in the tropics and the urgency to detect and monitor deforestation, fires and their emissions. Operational programmes to detect fires already exist (Setzer and Pereira 1991 b) or are being proposed (Frederiksen *et al.* 1990, Malingreau 1990) and spectral studies of the targets will certainly improve the methods in use or under consideration.

2. Materials

Full spatial resolution Advanced Very High Resolution Radiometer (AVHRR) images on channels 1, 2 and 3 from the NOAA-9 Sun-synchronous satellite (Kidwell 1985) were recorded from 26 July to 9 August 1985, at the HRPT (High Resolution Picture Transmission) tracking and receiving station of the Brazilian National Institute for Space Research (INPE) located at Cachoeira Paulista, SP (Lat 22°40' S Long 45°01' W), see table 1.

Table 1. NOAA-9/AVHRR images of 1985 used in the study.

Date	Orbit no.	Equatorial crossing	
		Hour, GMT	Longitude
19 July	3094	18 h18'43"	57-62°W
20 July	3108	18 h07'55"	54-91°W
21 July	3122	17 h57'06"	52-19°W
26 July	3193	18 h45'09"	64-15°W
27 July	3207	18 h34'20"	61-04°W
29 July	3235	18 h12'43"	55-96°W
31 July	3263	17 h51'06"	50-52°W
5 August	3334	18 h38'06"	65-61°W
6 August	3348	18 h28'11"	57-79°W
7 August	3362	18 h17'22"	57-07°W
9 August	3390	17 h55'45"	51-64°W

Picture element (pixel) sizes vary from the nominal nadir resolution of 1.1 km by 1.1 km to a maximum of about 2.4 km by 6.9 km at the off-nadir border of the image, when the scan angle reaches the maximum of 55.4° for the 1024th pixel. The channels recorded covered the optical spectrum in the $0.58\text{--}0.68\ \mu\text{m}$ (visible light), $0.72\text{--}1.1\ \mu\text{m}$ (near-infrared) and $3.55\text{ to }3.93\ \mu\text{m}$ (medium-infrared). Digital recording was made using only the eight most significant bits out of the ten existing in the radiometric resolution. Channel 4 ($10.3\text{ to }11.3\ \mu\text{m}$) and 5 ($11.5\text{ to }12.4\ \mu\text{m}$) were not recorded due to technical limitations of the station at that time. The information in these channels is probably not relevant for this study since they detect little energy from fires as pointed by Matson *et al.* (1984), and also because detection of regular clouds is possible also in channel 2. A strip of 100 pixels on each border of the images was disregarded to avoid analysis of highly geometrically distorted pixels. No atmospheric correction was made to account for different viewing angles of the AVHRR. The ascending orbit images used are listed in table 1 and were part of the images recorded for the fire detection programme of INPE (Setzer and Pereira 1991 b). Full resolution image processing was carried out in an 'Image-100' ('I-100') multi-spectral image analyser (GE 1975). The images were analysed in sectors of 512 by 512 pixels to match the I-100 maximum resolution and avoid sampling or repetition of pixels in the digital processing. The softwares used were 'histogram' to obtain distribution of digital counts, 'cluster synthesis' to allocate pixels in predetermined multi-spectral classes and the 'single cell' classifier to obtain statistics for classes of interest. 'Stretching' was used to produce enhanced images for visual interpretation and for photographing.

3. Results and discussion

Figure 1 shows digital counts in a scale of 256 levels for pixels in three AVHRR channels for a region near Carajas, PA, as registered in the 7 August image. The area limited by the continuous line in the centre corresponds to a site burning when the image was obtained; this area is also shown in the pair of pictures in figure 2, at about 9°S and $50\text{--}75^\circ\text{W}$. The evidence considered to associate active fires to this area was the presence of smoke in channels 1 and 2 originating from the same area. This same evidence was found for all other areas classified as burning sites. The digital counts for the hot or 'fire pixels' in thermal channel 3, from 1 to 12 (1 corresponding to the hottest possible temperature), are about one order of magnitude smaller than surrounding pixels associated to vegetation, with counts up to 149. Counts between 39 and about 100 possibly correspond to areas already burned or starting to burn at the time the image was acquired.

In channels 1 and 2 the pixels in the site can also be distinguished from the surrounding pixels, but not as evidently as in channel 3. In channel 2 pixels in the burning site, not covered by too much smoke, had counts between 30–37, only about 20 per cent less than pixels in the surrounding areas. Pixels covered by dense smoke had counts of 50–78 inside the site, and up to 126 to the west of the site, and therefore above the counts of the vegetation. Correspondingly, for channel 1 the values were 30–35, or 25 per cent higher for pixels with not much smoke, 45–81 for pixels with smoke in the site and up to 134 outside the site.

The above situation results largely from the high emission of energy by fires and by the transparency of smoke and of the atmosphere in the wavelengths of channel 3 in comparison to channels 1 and 2. As calculated by Robinson (1991), fires between 825–1000 K. have the peak of spectral emission from $3.5\text{--}2.9\ \mu\text{m}$, with an energy

CHANNEL 1

54	49	45	43	32	42	43	33	31	31	29	27	25	24	30	36	25
58	68	81	51	54	89	85	65	44	33	38	29	24	24	27	29	29
72	110	110	59	66	112	121	103	69	92	104	48	28	36	37	28	26
102	134	107	64	75	117	130	93	71	93	55	30	27	29	26	24	25
82	105	83	78	64	71	76	54	48	50	35	33	29	24	24	28	37
67	72	64	70	62	74	78	55	58	60	36	33	30	26	28	43	67
46	50	57	52	67	93	81	52	64	57	35	42	49	39	34	32	44
43	46	42	39	53	63	45	33	32	27	26	37	40	32	28	27	32
35	34	31	30	30	28	26	26	26	25	27	29	38	38	28	30	33
34	30	30	30	30	29	28	28	28	27	25	24	23	23	26	30	34
32	32	34	34	31	29	29	31	33	27	24	23	23	24	28	33	37

CHANNEL 2

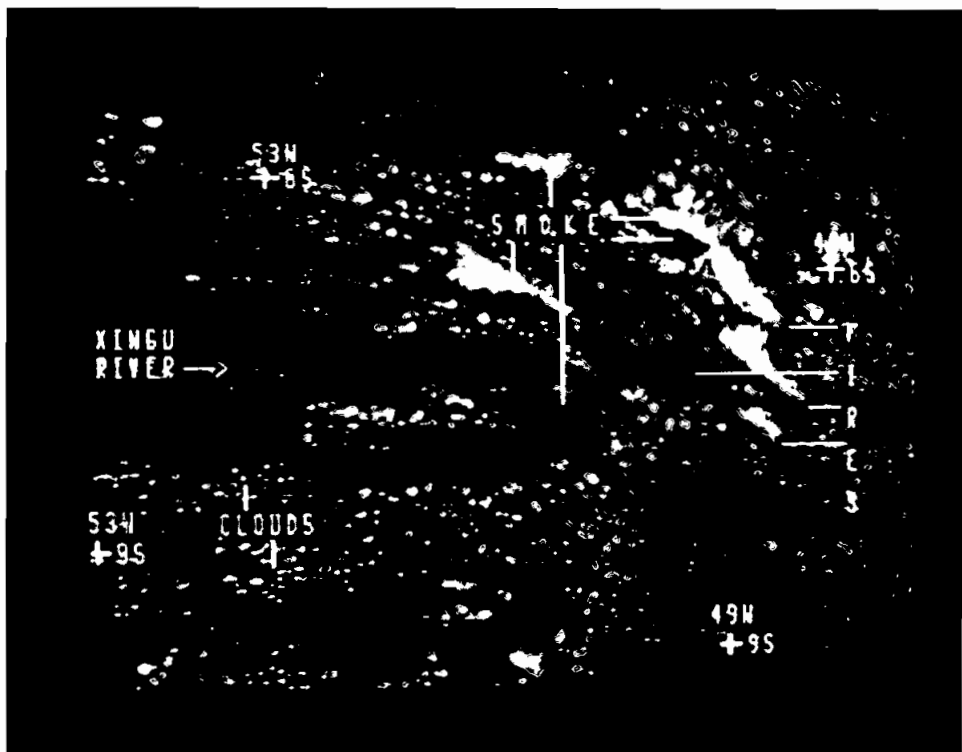
52	47	44	41	46	56	57	48	46	42	39	40	40	40	47	53	49
55	63	77	55	58	87	84	69	52	43	47	42	38	40	44	45	49
66	102	104	59	64	105	115	99	70	91	102	57	41	48	49	42	40
96	126	100	62	71	110	121	87	67	87	55	38	39	40	37	42	44
76	98	77	74	60	65	71	48	42	45	32	33	35	37	41	48	52
62	66	58	65	56	68	73	50	53	57	34	34	38	43	45	56	73
43	45	52	47	62	90	78	48	59	56	36	45	56	52	49	45	50
42	42	39	35	50	60	41	30	30	26	30	42	46	44	42	39	40
37	34	30	31	31	26	26	31	33	33	40	41	46	49	44	46	47
40	33	34	39	39	36	36	39	40	41	43	42	36	34	40	46	49
38	39	43	44	41	39	39	41	44	43	42	41	40	41	45	46	47

CHANNEL 3

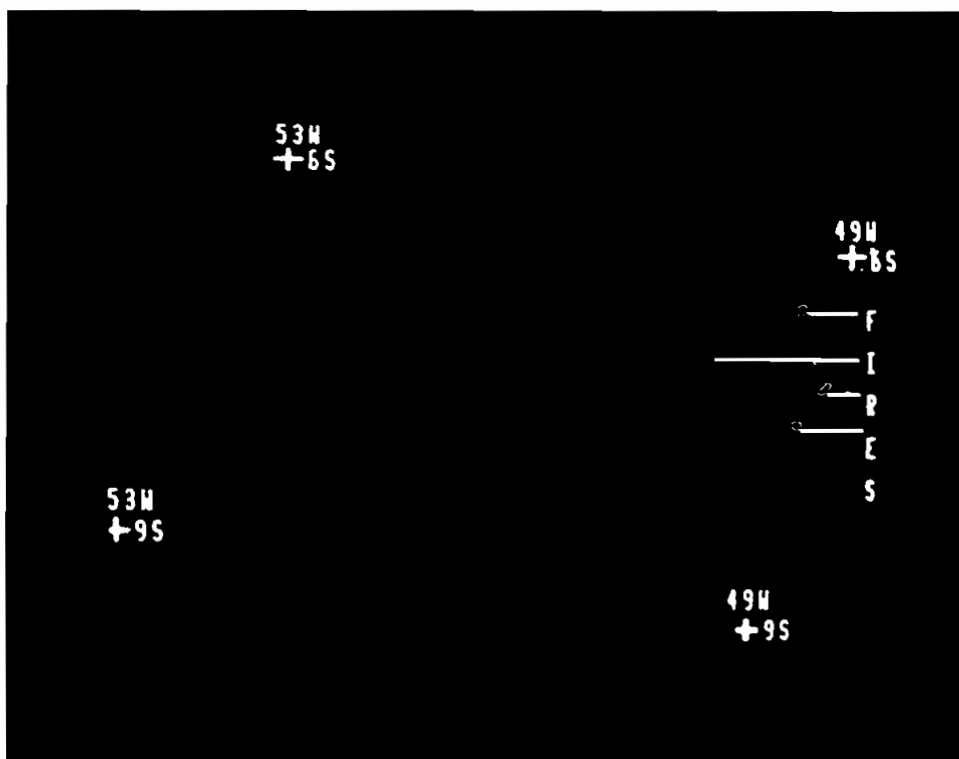
137	144	149	147	136	120	123	127	119	122	135	133	133	131	124	129	136
133	118	102	136	116	82	94	96	117	122	120	127	132	126	124	132	121
120	80	93	135	115	84	83	103	109	67	77	109	104	85	105	135	135
94	85	111	130	109	89	91	97	67	39	8	8	8	42	124	153	152
112	107	126	106	108	109	129	8	8	8	8	8	12	4	121	120	107
121	130	128	111	105	78	5	8	8	8	8	8	8	5	100	91	100
134	133	122	133	93	71	8	8	8	8	8	8	1	76	103	120	121
129	152	140	134	2	8	8	8	8	8	8	12	82	108	126	131	133
115	122	133	116	49	47	102	100	90	98	97	97	90	109	132	152	132
109	107	109	110	97	99	91	85	86	94	113	122	130	137	132	150	134
117	101	96	100	93	97	87	75	84	106	123	125	127	127	126	152	130

Figure 1. Digital counts for hot (fire) pixels in AVHRR channels 1, 2 and 3 on the NOAA-9 image of 7 August 1985. The area limited by the continuous line is a site burning.

Figure 2(a) Colour composition of AVHRR channels 1, 2 and 3 for geometrically uncorrected NOAA-9 image of 7 August 1985 showing active fires, smoke clouds and fair-weather cumulus clouds. (b) Digital classification of AVHRR channel 3 showing hot (fire) pixels for the same region shown in figure 2(a). Only pixels with digital counts from 1 to 8 are shown.



(a)



(b)

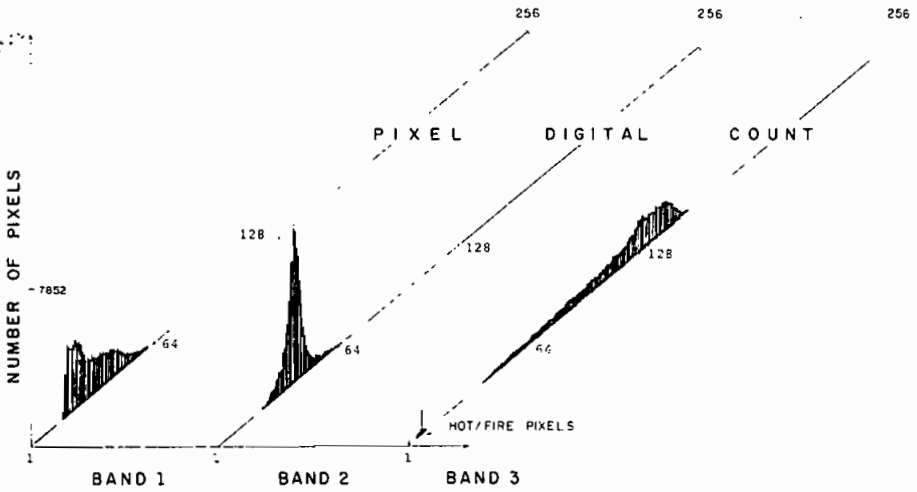


Figure 3. Histogram of pixel distribution in three AVHRR channels for 512 by 512 pixels of the NOAA-9 image of 9 August 1985. Note isolated peak in channel 3 associated to hot (fire) pixels.

amplification over the background of 3900–8900 times. For AVHRR channel 4 (10.3–11.3 μm), not used in this study, and also according to Robinson (1991) the amplification over the background is 25–37 times, much lower than in channel 3. Channels 1 and 2 proved to be highly susceptible to smoke emissions which are unavoidable in forest fires, and therefore impair the use of these channels in fire detection.

Figure 3 shows the histograms for the digital counts in channels 1, 2 and 3 for a region of 512 by 512 pixels in South of Pará State, on 9 August. Of the three histograms, the one for channel 3 shows an isolated concentration of pixels with low counts and which were identified as hot/burning sites. The identification was possible with the help of the image in the visible channel depicting smoke plumes originating from the same pixels. Figure 4 shows a more detailed enlargement of the histogram for channel 3, in which the peak for count levels in the one to eight range associated to the fire pixels is clear.

Table 2 presents means and standard deviations for pixel counts in three channels for 2544 saturated pixels with count level one and for 14832 pixels in the one to eight count range. These pixels were all associated to active fires in the fourteen sectors of 512 by 512 pixels extracted from all images used in this study. Also in these sectors, the visible channel was used to confirm the fires by showing dense smoke clouds originating from all the pixels selected.

The column Δ shows the count level range of fire pixels for various sectors of the images analysed. When this range is either just one or one to eight for channel 3, the corresponding range for bands one and two refers to those same pixels of channel 3. The next two columns in the table show the means and variances of the ranges, and the n column shows the number of pixels in the sector of 512 by 512 pixels analysed in the three channels.

The data shows that fire pixels are better defined in channel 3 than in channels 1 and 2 when one considers the count range as well as the means and variances. Fire

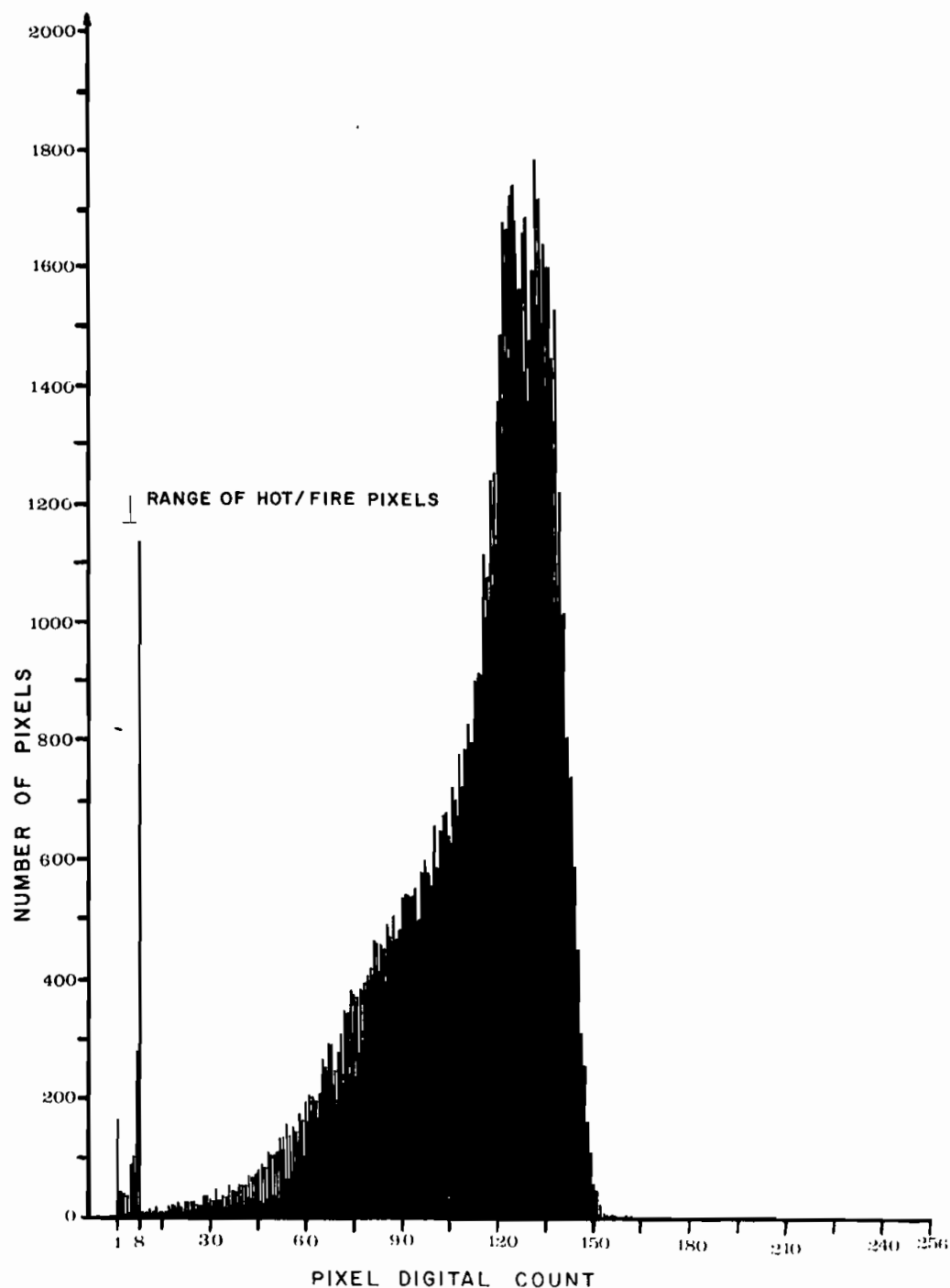


Figure 4. Detailed histogram of AVHRR channel 3 pixels shown in figure 3. Note that the peak related to hot (fire) pixels includes only 8 levels (in an 8-bit/256 scale) with higher frequency in the 8th level.

Table 2. Data and statistics of hot (fire) pixels, in AVHRR images. n is the number of hot (fire) pixels in the three channels; Δ , \bar{X} , S^2 , are respectively the ranges, averages and variances of the pixels in each range of digital counts.

Image date	Channel	Statistics—1st count of channel 3				Statistics—8 initial counts of channel 3				
		Δ	\bar{X}	S^2	n	Δ	\bar{X}	S^2	n	
26 July	3	1	1.0	0.0	22	1-8	6.1	6.8	166	
	2	30-70	41.1	112.7		26-97	36.7	86.4		
	1	22-71	31.9	183.0		20-100	30.4	140.2		
	3	1	1.0	0.0	27	1-8	5.2	7.9		133
	2	23-48	30.9	35.0		21-89	34.2	90.3		
	1	18-45	24.8	34.5		16-86	27.3	104.7		
29 July	3	1	1.0	0.0	32	1-8	6.4	6.7	230	
	2	15-71	35.4	120.7		15-71	35.6	89.5		
	1	14-71	27.6	166.2		14-71	26.6	128.7		
6 August	3	1	1.0	0.0	54	1-8	6.3	5.8	511	
	2	31-100	47.7	250.5		23-119	48.9	249.9		
	1	21-98	42.0	371.0		18-122	43.4	367.1		
7 August	3	1	1.0	0.0	98	1-8	6.6	5.5	985	
	2	24-72	36.8	96.2		24-72	36.9	53.7		
	1	16-79	29.3	131.4		16-79	28.6	99.2		
	3	1	1.0	0.0	120	1-8	6.3	6.0		1051
	2	17-128	45.7	212.3		17-128	45.3	170.7		
	1	17-125	39.5	290.6		17-125	40.5	251.2		
9 August	3	1	1.0	0.0	1020	1-8	5.3	8.1	4641	
	2	23-112	38.4	70.1		17-123	39.2	91.6		
	1	20-107	32.1	90.2		16-127	34.3	139.2		
	3	1	1.0	0.0	32	1-8	6.8	5.0		386
	2	19-82	41.2	195.9		19-82	39.5	115.9		
	1	18-88	36.1	305.4		18-88	32.9	188.4		
	3	1	1.0	0.0	74	1-8	6.8	4.9	877	
	2	23-82	41.4	131.9		19-88	39.3	93.7		
	1	19-88	36.3	239.4		17-91	33.8	173.4		
	3	1	1.0	0.0	22	1-8	6.5	6.0		184
	2	27-122	68.8	1386.8		20-125	48.5	662.4		
	1	22-125	64.5	1830.0		19-128	41.4	851.8		
	3	1	1.0	0.0	54	1-8	6.7	4.6	729	
	2	29-100	41.1	129.5		22-123	40.1	72.3		
	1	2-105	37.9	192.8		17-127	37.8	128.3		
	3	1	1.0	0.0	765	1-8	5.0	8.4		3061
	2	22-103	41.0	54.5		17-114	40.9	76.2		
	1	20-109	33.8	76.5		16-119	34.3	123.9		
	3	1	1.0	0.0	79	1-8	6.7	5.0	924	
	2	21-82	39.9	111.1		19-88	38.5	89.5		
	1	19-88	34.6	205.0		16-91	33.1	165.9		
3	1	1.0	0.0	145	1-8	6.0	6.8	954		
2	16-98	33.0	155.9		17-98	38.0	92.7			
1	16-107	30.4	178.4		16-103	34.2	152.5			

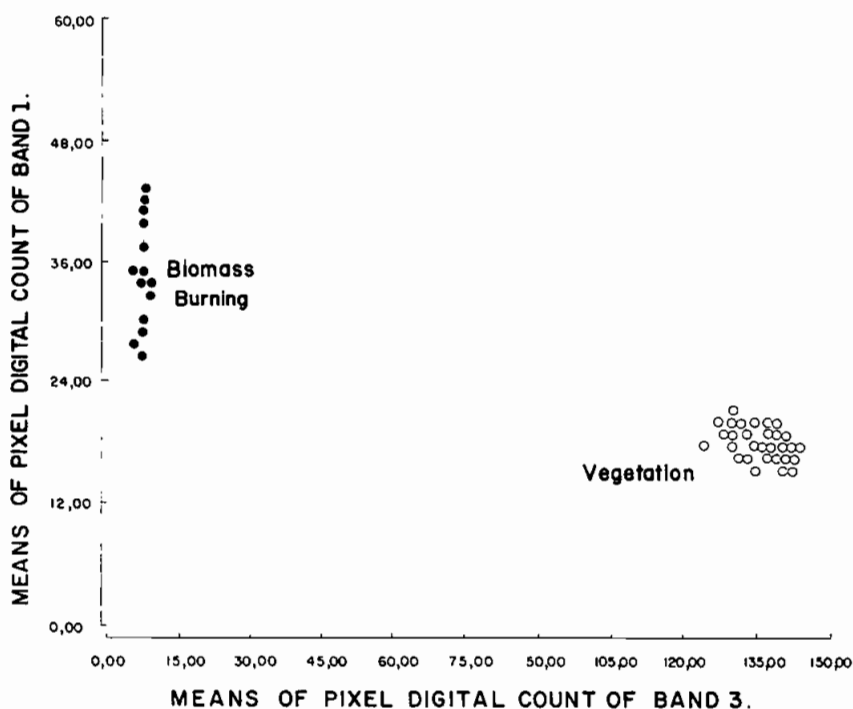


Figure 5. AVHRR channels 1 and 3 bi-spectral distribution of active fires and vegetation. Each of the 14 fire and 30 vegetation dots actually represent averages for the sectors given in tables 1 and 2.

pixels presented mean counts between 5.2 (26 July) and 6.8 (9 August) with a maximum variance of 8.4 (9 August) when using the one to eight count limit. Ranges for the other channels were much wider and consequently variances were also higher, indicating that channel 3 provides a much more defined range to detect hot pixels. For channel 1, the means in the column with statistics for the eight initial counts (in channel 3) varied from 26.6 (29 July) to 43.4 (6 August). The variances, in the same column of statistics, varied from 99.2 (7 August) to 851.9 (9 August).

The wider variances and ranges of count values of fire pixels in channels 1 and 2 can be explained by the effect of the smoke produced by the fires and by differences in ground covers. The smoke increases the reflection of incoming solar radiation and also diffuses the outgoing radiation reflected by the different ground covers. Concerning ground covers, the areas burning at the time the satellite images were obtained naturally had different amounts of exposed soil and content of ashes, reflecting more solar radiation, and therefore increasing the range in the count values in these two channels.

Figure 5 shows on a bi-spectral graph for channels 1 and 3 that fire and vegetation pixels are well separated without possibility of confusion. Each point in the graph is actually the average of many samples obtained from the eleven images already listed in table 1. Details of the vegetation samples plotted in figure 5 are given in table 3, and were always from dense tropical forest areas and less polluted by smoke; the points for biomass burning represent the average counts of the hot

Table 3. Data and statistics for samples of vegetation pixels in AVHRR images. n is the number of pixels in the three channels. Δ , \bar{X} , S^2 , are respectively the ranges, averages and variances of the pixels. The 'total' column refers to all samples in each image combined.

Image date	Channel	Radiometric range	Mean	S^2	n	Total mean	N
19 July	1	15-18	15.1	0.1	2100	15.3 34.7 140.1	2200
	2	32-37	34.3	0.6			
	3	129-144	140.2	2.0			
	1	19-21	19.6	0.3	100		
	2	40-44	42.1	0.6			
	3	136-143	138.8	1.8			
20 July	1	16-26	16.6	3.3	36	18.0 41.4 136.1	920
	2	39-47	40.4	2.1			
	3	120-143	140.3	15.4			
	1	18-18	18.0	0.0	884		
	2	39-47	41.4	0.7			
	3	120-143	136.0	3.7			
21 July	1	16-18	16.7	0.2	196	15.5 35.9 140.3	1132
	2	35-40	38.0	1.0			
	3	134-139	136.4	1.0			
	1	15-16	15.2	0.1	836		
	2	33-38	35.4	0.8			
	3	135-148	141.3	2.7			
	1	15-16	15.3	0.2	100		
	2	34-37	35.4	—			
	3	137-147	140.2	—			
26 July	1	19-20	19.0	0.1	100	19.3 1.0 138.3	276
	2	40-44	42.2	0.8			
	3	137-141	138.7	0.6			
	1	19-20	19.4	0.2	140		
	2	41-46	42.9	0.7			
	3	135-141	138.3	1.2			
	1	20-20	20.0	0.0	36		
	2	43-45	44.2	0.3			
	3	135-139	136.8	1.0			
27 July	1	19-20	20.0	0.0	324	19.5 43.1 136.5	604
	2	41-46	43.1	0.7			
	3	133-140	136.7	1.5			
	1	19-20	19.0	0.0	220		
	2	42-45	42.9	0.6			
	3	133-139	136.3	1.3			
	1	17-20	18.9	0.3	60		
	2	42-46	43.9	0.9			
	3	133-140	136.2	2.3			
29 July	1	17-18	17.3	0.2	100	17.3 42.6 135.0	848
	2	40-43	41.3	0.4			
	3	129-134	131.6	1.2			
	1	17-20	17.3	0.2	748		
	2	38-48	42.7	2.5			
	3	125-143	135.8	7.4			

Table 3 *continued*

Image date	Channel	Radiometric range	Mean	S ²	<i>n</i>	Total mean	<i>N</i>
31 July	1	16-18	16.6	0.3	100	16.7 37.0 135.8	460
	2	36-39	37.6	0.3			
	3	133-138	135.0	1.1			
	1	16-19	17.4	0.4	60		
	2	32-40	38.2	1.6			
	3	111-141	138.8	31.0			
	1	17-18	17.1	0.1	60		
	2	36-39	37.9	0.8			
	3	136-141	138.8	1.7			
	1	16-17	16.0	0.0	100		
	2	35-39	36.6	0.9			
	3	129-141	133.5	5.0			
	1	16-21	16.7	0.9	140		
	2	32-42	36.2	2.4			
	3	126-143	138.4	8.1			
5 August	1	17-17	17.0	0.0	156		
	2	34-38	36.3	1.1			
	3	139-148	142.5	1.9			
	1	17-18	17.9	0.1	36		
	2	35-36	35.8	0.1			
	3	134-142	139.1	2.4			
	1	17-18	17.5	0.3	140		
	2	31-36	34.4	0.6			
	3	136-144	140.7	2.0			
	1	18-21	18.1	0.2	140		
	2	33-37	35.0	0.2			
	3	134-148	141.8	2.8			
	1	18-18	18.0	0.0	84		
	2	34-35	35.0	0.0			
	3	140-148	142.9	—			
	1	19-20	19.9	0.1	36		
	2	42-45	43.4	0.6			
	3	132-135	133.1	0.9			
	1	19-23	20.0	0.2	100		
	2	34-39	36.3	0.9			
	3	130-143	136.1	5.7			
6 August	1	19-20	19.9	0.1	36		
	2	42-44	43.3	0.3			
	3	132-136	133.9	0.6			
	1	20-21	20.9	0.1	36		
	2	44-47	45.2	0.6			
	3	116-130	126.4	7.7			
	1	19-23	19.9	0.8	484		
	2	40-47	43.3	1.8			
	3	129-144	137.3	6.7			
	1	20-23	20.5	0.6	36		
	2	43-47	45.3	0.7			
	3	121-129	126.1	2.6			
	1	20-23	21.1	0.2	60		
	2	43-46	44.8	0.6			
	3	125-133	128.3	2.2			

Table 3 continued

Image date	Channel	Radiometric range	Mean	S ²	n	Total mean	N
7 August	1	20-21	20.7	0.2	36	20.2	688
	2	44-46	45.1	0.3			
	3	128-132	130.1	0.9			
	1	20-22	20.2	0.2	60		
	2	44-49	46.4	1.0			
	3	125-132	128.9	2.7			
	1	18-21	19.3	0.3	60		
	2	35-46	42.9	4.2			
	3	126-136	129.1	3.6			
1	19-19	19.0	0.0	60			
2	40-45	42.6	1.1				
3	125-131	128.4	1.7				
1	19-20	19.0	0.0	60			
2	40-46	42.2	1.0				
3	113-132	127.1	12.2				
1	18-21	19.1	0.1	192			
2	31-45	42.4	2.5				
3	121-138	128.9	—				
1	18-20	18.6	0.3	684			
2	35-41	38.1	0.8				
3	127-136	133.2	2.2				
1	18-19	18.4	0.2	180			
2	37-42	38.3	0.7				
3	130-139	135.5	3.3				
1	16-19	17.2	0.2	1140	18.0	2436	
2	34-43	37.3	2.1				
3	120-143	137.2	7.2				
9 August	1	16-22	17.7	0.4	140		
	2	36-41	37.7	0.8			
	3	117-141	133.8	6.8			
	1	18-19	18.4	0.2	100		
	2	35-38	37.2	0.6			
	3	123-134	128.9	5.3			
	1	19-21	19.1	0.2	36		
	2	34-49	43.2	5.6			
	3	128-138	131.5	4.1			
	1	18-19	18.2	0.2	60		
	2	42-44	42.5	0.5			
	3	114-127	123.2	4.2			
	1	18-19	18.0	0.0	140	18.2	1496
	2	35-39	37.8	0.5			
	3	114-140	134.0	1.5			

pixels in the one to eight range from table 2. Vegetation samples in channel 3 had low average values of counts, ranging from 123.2 (9 August) to 142.9 (5 August), and were more than one order of magnitude higher than the biomass burning pixel counts. (It must be remembered that channel 3 has an inverted scale, where the

Table 4. AVHRR response in channels 1, 2 and 3 for active fires, smoke and vegetation. Values represent averages obtained from many sectors and images referenced in tables 1, 2 and 3. Intervals of confidence refer to the significance level of 1 per cent ($\alpha=0.01$).

Channel	Fire	Forest	Smoke
1	34 ± 34	17 ± 1	39 ± 8
2	40 ± 28	38 ± 3	44 ± 5
3	6 ± 7	137 ± 5	136 ± 31

lowest count values correspond to highest energy levels received by the AVHRR sensor.) The difference between counts of fire and vegetation pixels in channel 2 did not exist, since in this channel average counts of pixels ranged from 34.2 (26 July) to 48.9 (6 August) for fire pixels (table 2), and from 34.3 (19 July) to 46.4 (7 August) for forest pixels (table 3). For channel 1, the counts varied from 26.6 (29 July) to 43.4 (6 August) for fire pixels (table 2), and from 15.1 (19 July) to 21.1 (6 August) for forest pixels, making the difference in this channel barely marginal to separate these two classes. Therefore fires are better distinguished from surrounding forest in channel 3, and to some extent also in channel 1. With the presence of significant amounts of smoke, channel 1 will also record reflected radiation from the smoke particles, preventing the recording of good data of the forest cover, and consequently making its use unreliable for fire detection in typical conditions of biomass burning in the forest.

The above information can be summarized in table 4, where average count values for all samples of fire and forest pixels combined are presented. Average data of samples of pixels on downwind dense smoke plumes over forest background has also been included; for more details about the characteristics of this class (smoke) see Pereira (1988). In channel 3, forest and smoke had close responses, indicating that in the $3.7 \mu\text{m}$ wavelength the smoke does not show high temperatures and that it can be penetrated to a large extent. In channel 2 the three classes had responses relatively close, again indicating that this channel is not appropriate to fire detection. In channel 1 smoke had higher count levels than forests and to some extent than fires, corroborating the likelihood that it reflects incoming solar radiation, and therefore that it interferes in the detection of fires in real biomass burning conditions.

4. Conclusions

Digital analysis of channels 1, 2 and 3 of NOAA-9 AVHRR images indicated that channel 3 ($3.55\text{--}3.93 \mu\text{m}$) is the best one to detect active fires in a region of tropical forests. Channels 1 and 2 are subject to effects of smoke and cause the fires to be mistaken with other ground covers. Channel 3 showed pixels with digital counts of more than one order of magnitude smaller than for other ground covers. Most fires were found in the 8th count (in 256 levels, or 32nd on 1024 levels) and not in the saturated level. Data about biomass burning in tropical forests is becoming increasingly important to study the carbon cycle and atmospheric contamination in general. The simple technique to detect fires based on AVHRR/HRPT channel 3, and the relatively low costs of image reception and processing presents therefore a strong potential to assess occurrences of fires in near-real time.

Acknowledgments

The financial support of Conselho Nacional de Desenvolvimento Científico e Tecnológico (CNPq) and Fundação de Amparo à Pesquisa do Estado de SP (FAPESP) as well as the technical support from LTID and DOP departments of INPE is highly acknowledged.

References

- ANDREAE, M. O., BROWELL, E. V., GARSTANG, M., GREGORY, G. L., HARRIS, R. C., HILL, G. F., JAQCOB, D. J., PEREIRA, M. C., SACHSE, G. W., SETZER, A. W., DIAS, P. L. S., TALBOT, R. W., TORRES, A. L., and WOFSY, S. C., 1988, Biomass burning emission and associated haze layers over Amazonia. *Journal of Geophysical Research*, **93**, 1509–1527.
- CHUNG, Y.-S., and LE, H. V., 1984, Detection of fire smoke plumes by satellite imagery. *Atmospheric Environment*, **18**, 2143–2151.
- CRUTZEN, P. J., and ANDREAE, M. O., 1990, Biomass burning in the tropics: Impact on atmospheric chemistry and biogeochemical cycles. *Science*, **250**, 1669–1678.
- DOZIER, J., 1981, A method for satellite identification of surface temperature fields of subpixel resolution. *Remote Sensing of Environment*, **11**, 221–229.
- EOSAT, 1988, The Yellowstone wildfires of 1988. *Landsat Data Users Notes*, **3**, p. 12.
- ERNST, J. A., and MATSON, M., 1977, A NOAA-5 view of Alaskan smoke patterns. *Bulletin of the American Meteorological Society*, **58**, 1074–1076.
- FLANNIGAN, M. D., 1985, Forest fire monitoring using the NOAA satellite series. MSc Thesis, Colorado State University, Fort Collins, CO.
- FLANNIGAN, M. D., and HAAR, T. H. V., 1986, Forest fire monitoring using the NOAA satellite series. In *American Meteorological Society Symposium, Atlanta, Georgia* (Atlanta: A.M.S.), pp. 168–172.
- FREDERIKSEN, P., LANGAAS, S., and MBAYE, M., 1990, NOAA-AVHRR and GIS-based monitoring of fire activity in Senegal—a provisional methodology and potential applications. In *Fire in the Tropical Biota*, edited by J. G. Goldammer (Berlin: Springer-Verlag), pp. 400–417.
- G.E., GENERAL ELECTRIC COMPANY, 1975, *Image 100: User Manual* (Daytona Beach, Florida: G.E.).
- KAUFMAN, Y. J., SETZER, A. W., JUSTICE, C., TUCKER, C. J., PEREIRA, M. C., and FUNG, I., 1990, Remote sensing of biomass burning in the tropics. In *Fire in the Tropical Biota*, edited by J. G. Goldammer (Berlin: Springer-Verlag), pp. 371–399.
- KIDWELL, K. B., 1985, NOAA polar orbiter data (TIROS-N, NOAA-6, NOAA-8 and NOAA-9) user guide. NOAA-NESS, Washington, DC.
- KIRCHHOFF, V. W. J. H., SETZER, A. W., and PEREIRA, M. C., 1989, Biomass burnings in Amazonia: seasonal effects on atmospheric O₃ and CO. *Geophysical Research Letters*, **16**, 469–472.
- LEE, T. F., and TAG, P. M., 1990, Improved detection of hotspots using the AVHRR 3.7 μm channel. *Bulletin of the American Meteorological Society*, **71**, 1722–1730.
- MALINGREAU, J. P., 1984, Remote sensing and disaster monitoring: a review of application in Indonesia. *International Symposium on Remote Sensing of Environment*, **18**, Paris, France. Proceedings of E.R.I.M. (Ann Arbor: E.R.I.M.), **1**, pp. 283–297.
- MALINGREAU, J. P., 1990, The contribution of remote sensing to the global monitoring of fires in tropical and subtropical ecosystems. In *Fire in the Tropical Biota*, edited by J. G. Goldammer (Berlin: Springer-Verlag), pp. 337–370.
- MALINGREAU, J. P., STEPHENS, G., and FELLOWS, L., 1985, Remote sensing of forest fires: Kalimantan and North Borneo in 1982–83. *Ambio*, **14**, 314–321.
- MATSON, M., and DOZIER, J., 1981, Identification of subresolution high temperatures sources using thermal IR sensor. *Photogrammetric Engineering and Remote Sensing*, **47**, 1311–1318.
- MATSON, M., and HOLBEN, B., 1987, Satellite detection of tropical burning in Brazil. *International Journal of Remote Sensing*, **8**, 509–516.
- MATSON, M., SCHNEIDER, S. R., ALDRIDGE, B., and SATCHWELL, B., 1984, Fire detection using the NOAA-series satellites. NOAA-NESS, Washington, DC (NOAA-TR-NESDIS-7).

- MATSON, M., STEPHENS, G., and ROBINSON, J., 1987, Fire detection using data from the NOAA-N satellites. *International Journal of Remote Sensing*, **8**, 961-970.
- MUIRHEAD, K., and CRACKNELL, A. P., 1985, Straw burning over Great Britain detected by AVHRR. *International Journal of Remote Sensing*, **6**, 827-833.
- PEREIRA, M. C., 1988, Detection, monitoring and analysis of some environmental effects of biomass burnings in Amazon region using NOAA and Landsat satellite images, and airborne data. MSc Thesis in Remote Sensing (in Portuguese), INPE, São Jose dos Campos, SP, Brazil, 268pp. (INPE-4503-TDL/362).
- ROBINSON, J. M., 1991, Fire from space: Global fire evaluation using infrared remote sensing. *International Journal of Remote Sensing*, **12**, 3-24.
- SETZER, A. W., and PEREIRA, M. C., 1991 a, Amazônia biomass burning in 1987 and an estimate of their tropospheric emissions. *Ambio*, **20**, 19-22.
- SETZER, A. W., and PEREIRA, M. C., 1991 b, Operational detection of fires in Brazil with NOAA-AVHRR. *24th International Symposium on Remote Sensing of the Environment, Rio de Janeiro, Brazil* (Ann Arbor: E.R.I.M.). In Press.
- SETZER, A. W., KIRCHHOFF, V. W. J. H., and PEREIRA, M. C., 1991, Ozone concentrations in the Brazilian Amazonia during BASE-A. In *Global Biomass Burning—Proceedings Chapman Conference*, edited by J. Levine (Boston: MIT Press), pp. 112-114.
- SVEJKOVSKY, J., 1985, Santa Ana airflow observed from wildfire smoke patterns in satellite imagery. *Monthly Weather Review*, **113**, 902-906.